Acta Astronautica 199 (2022) 174–182

Contents lists available at ScienceDirect

Acta Astronautica

journal homepage: www.elsevier.com/locate/actaastro

Effects of swirl injection on the combustion of a novel composite hybrid rocket fuel grain

Zelin Zhang [a,b], Xin Lin [a,c,*], Zezhong Wang [a], Kun Wu [a], Jiaxiao Luo [a,c], Sihan Fang [a,c], Chunyuan Zhang [b], Fei Li [a], Xilong Yu [a,c]

[a] State Key Laboratory of High Temperature Gas Dynamics, Institute of Mechanics, Chinese Academy of Sciences, Beijing, 100190, China
[b] College of Mechatronics Engineering, North University of China, Taiyuan, 030051, China
[c] School of Engineering Science, University of Chinese Academy of Sciences, Beijing, 100049, China

ARTICLE INFO

Keywords:
Hybrid rocket engine
Swirl injection
Novel composite fuel grain
Regression rate
Oxidizer-to-fuel ratio

ABSTRACT

The combustion characteristics obtained from the coupling effect between swirl injection and a novel composite hybrid rocket fuel grain were investigated. The novel composite fuel grain was composed of a three-dimensional printed acrylonitrile-butadiene-styrene (ABS) helical substrate with an embedded paraffin-based fuel. Two swirl flow injectors with opposite injection directions were designed: one with the same injection direction as the swirling direction induced by the ABS helical substrate and the other having the opposite direction. Axial injection trials were also performed as a baseline for comparison. Firing tests were carried out using a lab-scale hybrid rocket engine with oxygen as the oxidizer at average mass flux values in the range of 2.1–4.5 g/(s·cm^2). When combined with either swirl flow injector, the novel composite fuel grain exhibited excellent combustion properties. Compared with the axial flow injector, both swirl injectors greatly improved the regression rate of the novel composite fuel grain, by 82.4% and 50.6% respectively, at an oxygen mass flux of approximately 4.25 g/(s·cm^2). Three-dimensional imaging of the inner surface of the novel composite fuel grain and cold flow numerical simulations were employed to assess the mechanism by which the regression rate was increased. The results of these analyses elucidated the effects of different injection methods on the oxidizer-to-fuel ratio distribution during combustion of the novel composite fuel grain.

1. Introduction

Hybrid rocket engines (HREs) combine the inherent advantages of both liquid and solid rocket engines, such that they are generally safe and inexpensive while providing adjustable thrust and less complexity than conventional rocket engines [1–3]. As a result of these advantages, HREs are expected to have numerous applications in future [4–7]. However, primarily because of the inherent low fuel regression rate and oxidizer-to-fuel ratio (O/F) shift issues that are common to most conventional HREs, these engines have not yet been developed to the same extent as liquid and solid rocket engines. These issues must therefore be resolved for HRMs to be viable alternatives for practical applications.

Swirl injection has been proven to be an effective means of increasing the regression rates of fuel grains by increasing the turbulence intensity and promote heat transfer, enhancing the shear effect of heat flow on the fuel and increasing the heat flux density at the boundary layer [8–21]. Knuth et al. [8] first introduced swirl injection into an HRE by installing an injector between the fuel base and the converged section of the engine nozzle. Firing tests showed that the regression rate of a hydroxyl-terminated polybutadiene fuel was increased by a factor of 7 at a gaseous oxygen mass flux of 1 g/(cm^2·s) when using this system. Subsequently, Yuasa et al. [9] installed a swirl injector at the head of the engine to simplify the structure and carried out firing tests that showed a significant increase in the regression rate. During these trials, a highly turbulent swirl flow field was found to form in the engine combustion chamber based on observations with a quartz fiber spectroscopic system. Although this structure was both effective and practical [14,15,17], it caused an uneven regression rate distribution along the fuel grain in the axial direction. To address this issue, Ohyama et al. [10,11,13] proposed a multi-section swirl structure in which swirling flows were generated at several cross-sections along the combustion chamber. Firing tests demonstrated that this design gave a more consistent fuel grain regression rate with the increase of oxidizer injectors. However, this multi-section injection structure required an

* Corresponding author. State Key Laboratory of High Temperature Gas Dynamics, Institute of Mechanics, Chinese Academy of Sciences, Beijing, 100190, China.
E-mail address: linxin_bit@imech.ac.cn (X. Lin).

https://doi.org/10.1016/j.actaastro.2022.07.027
Received 1 March 2022; Received in revised form 24 June 2022; Accepted 17 July 2022
Available online 20 July 2022

extremely complicated piping system and resulted in serious erosion at the injection location [19].

Another attractive strategy is to design a fuel grain having a complex port shape that provides an effect similar to that of swirl injection [22–32]. With the recent progress in three-dimensional (3D) printing technology, an almost infinite range of fuel port shapes can now be easily manufactured. In one representative study, Whitmore et al. [22, 23] used fused deposition modeling to fabricate acrylonitrile-butadiene-styrene (ABS) fuel grains with helical port structures. The experimental analysis of these grains suggested that this structure increased the regression rate by as much as 3–4 times compared with straight-bore fuel grains under the same experimental conditions. Whitmore et al. also confirmed that this structure introduced centrifugal flow patterns into the combustion chamber, which were a primary cause of the increased regression rates. However, this special structure gradually disappeared as combustion progressed and the grain burned back, such that the regression rate enhancement was slowly weakened.

In prior work, our own group developed an ABS/paraffin-based composite fuel (A/PC) grain that maintained a swirl flow field during the entire combustion process [32]. This grain comprised an ABS helical substrate fabricated by 3D printing and an embedded paraffin-based fuel and was able to generate and maintain a nested helical structure during the combustion process because of the different regression rates of the two fuels. Experimental results indicated that the regression rate of this grain was significantly improved relative to that of a pure paraffin-based fuel (PP) grain, and that the regression rate could be further improved by increasing the oxygen mass flux. It was anticipated that combining this A/PC grain with a swirl flow injector could have a synergistic effect by which the regression rate would be further increased because of coupling between the nested helical morphology and the swirl injection.

The present work studied the combustion characteristics of an engine in which the coupling effect between swirl injection and an A/PC grain was achieved. Two types of swirl flow injectors were used to investigate the coupling effect, one of which generated a swirl flow field in the same direction as the swirling guided by the ABS helical substrate while the other generated a swirl flow in the opposite direction. Axial injection trials were also performed to provide a performance baseline for comparison with the coupling effect. Firing tests were carried out using lab-scale HREs with oxygen as the oxidizer at average mass flux values of 2.1–4.5 g/(s·cm^2), corresponding to combustion chamber pressures of 0.8–2.6 MPa. The combustion chamber pressure, grain regression rate, combustion efficiency and O/F distribution were all investigated during these trials and are discussed in detail herein. The inner surface of each A/PC grain was also imaged using a 3D laser scanner to qualitatively analyze the effect of different injection methods on the formation of the nested helical structure. In addition, a cold flow numerical simulation was carried to elucidate the mechanism by which the regression rate was increased when using an A/PC grain with a swirl flow injector. Variations in the O/F distribution caused by different injector methods were assessed and approaches to controlling this factor in hybrid rockets are examined herein based on the above analyses.

2. Experimental setup

2.1. Fuel grain design and manufacturing

The A/PC grain design concept and the manufacturing process used to fabricate these grains are shown in Fig. 1. The A/PC grain consisted of an ABS helical substrate formed by 3D printing with an embedded paraffin-based fuel. The helical structure was made of an outer wall with multiple spiral blades rotating counterclockwise in the axial direction and provided mechanical support to the paraffin-based fuel while also serving as an additional fuel. During combustion, the different regression rates of the two materials in the grain worked to maintain the nested helical structure composed of multiple grooves between adjacent ABS blades (Fig. 1a). The nested helical morphology induced a swirl flow field that corresponded to the helical direction of the ABS substrate with vortexes at the grooves between adjacent ABS blades. This swirl flow field brought the flame closer to the grain surface and strengthened the flow shear effect on the wall. In addition, the vortexes promoted the exchange of substances between the combustion zone and the fuel grain wall. Together, these various phenomena increased the regression rate of the grain.

The manufacture of the A/PC grain proceeded in two steps. First, an ABS helical substrate (Fig. 1b) was prepared using a 3D printer (Raise3D, N2 Plus). This structure contained nine spiral blades and had a length, outer diameter and inner diameter of 100, 60 and 20 mm, respectively. The ABS outer wall had a thickness of 2 mm. A molten paraffin-based fuel was cast into the substrate via a centrifugal process until all the gaps between the ABS blades were filled. This material was the main component of the A/PC grain, accounting for approximately 87% of the total mass (excluding the ABS outer wall). The resulting fuel grain is shown in Fig. 1c. The paraffin-based fuel and the blades formed a bore with a constant initial inner diameter and each trial used the same fuel grain inner diameter. The formulation of paraffin-based fuel and details of the process used to manufacture the A/PC grain can be found in previous publications [32–35].

2.2. Hybrid rocket engine structure and configurations

The lab-scale HRE used in this study is shown in Fig. 2. During these trials, gaseous oxygen was employed as the oxidizer and the fuel grain was ignited with a methane/oxygen torch activated by a conventional spark plug. The oxidizer injector and the igniter were located at the head of the engine. The mass flow rate of the oxidizer was in the range of 8–24 g/s and was adjusted by a calibrated mass flow controller (Bronkhorst, model F-203AV). These rates corresponded to average mass flux values of 2.1–4.5 g/(s·cm^2). The length of the combustion chamber was 100 mm and the inner diameter was 60 mm, both of which were consistent with the length and outer diameter of the fuel grain. After the firing tests, a 3D laser scanner (Hangdaqingyun Technology Co. Ltd., RayScan771) with a volume accuracy of 0.02 mm/m was used to image the inner surface of the grain.

The structures of the injectors are shown in detail in the red dashed

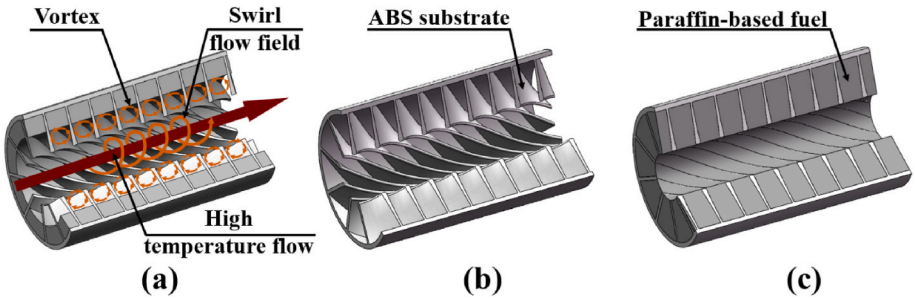

Fig. 1. a) Operational principle of the A/PC grain, b) the ABS substrate, and c) the manufactured A/PC grain.

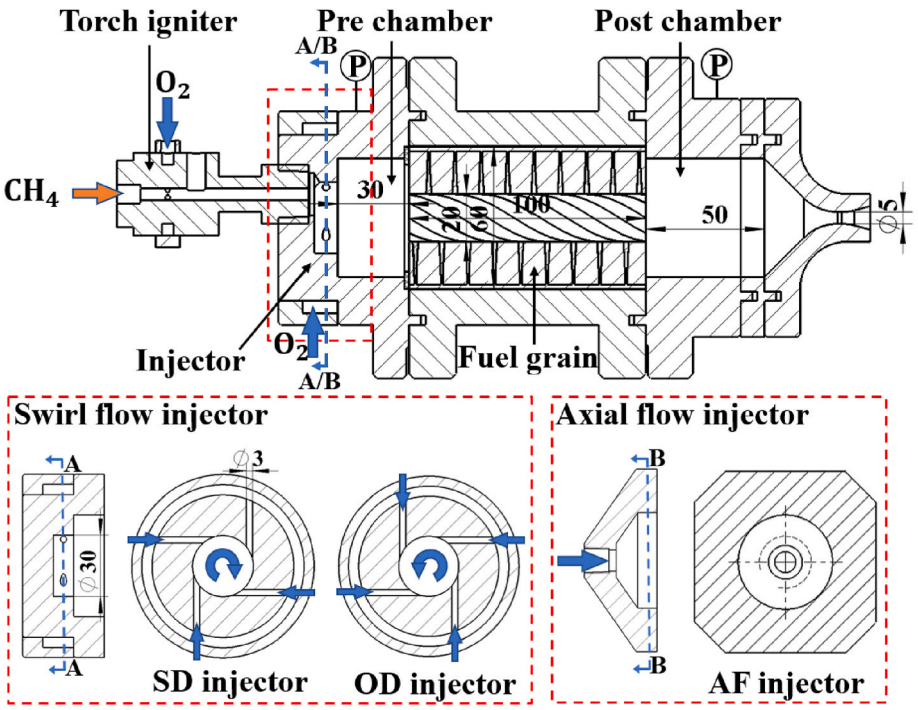

Fig. 2. Schematics of the lab-scale HRE and different injectors used in this work.

panels within Fig. 2. Two typical swirl flow injectors were designed for this work. One generated a swirl flow field moving in the same direction as the swirling motion induced by the ABS blades, and is referred to herein as the same direction (SD) injector. The second injector provided flow in the opposite direction and so is termed the opposite direction (OD) injector. The swirl number (S_g) could characterize the swirling intensity of the injector, and can be calculated through the method presented in Ref. [36]. The S_g of two swirl flow injectors numbers is all 22.5 but in opposite directions. An axial flow (AF) injector was also used in some trials for comparison purposes. The combustion characteristics of four engine configurations were studied: the SD injector coupled with an A/PC grain, the OD injector coupled with an A/PC grain, the AF injector coupled with an A/PC grain and the AF injector coupled with a PP grain.

2.3. Regression rate data processing methodology

Fig. 3 shows the schematic diagram of the A/PC grain cross-section before and after combustion. Owing to the complicated structure of the A/PC grains, the regression rates in this paper were calculated as average values, using the expression:

$$r_{rate} = \frac{r_f - r_0}{t_{burn}} \tag{1}$$

where t_{burn} is the burn time of the grain, r_0 is the initial radius of the fuel grain and r_f is the radius of the fuel grain after combustion. The latter term is obtained by weighing as

$$r_f = \sqrt{\frac{\frac{m_{f0}-m_f}{\rho_c} + V_0}{\pi L}} \tag{2}$$

where m_{f0} and m_f are the mass of the fuel grain before and after combustion, respectively, V_0 is the initial volume of the inner bore of the grain, L is the length of the grain and ρ_c is the average density of the grain. The A/PC grain density, ρ_c, was calculated as an average value for the two fuels, given by

$$\rho_c = \rho_p \omega_p + \rho_{ABS} \omega_{ABS} \tag{3}$$

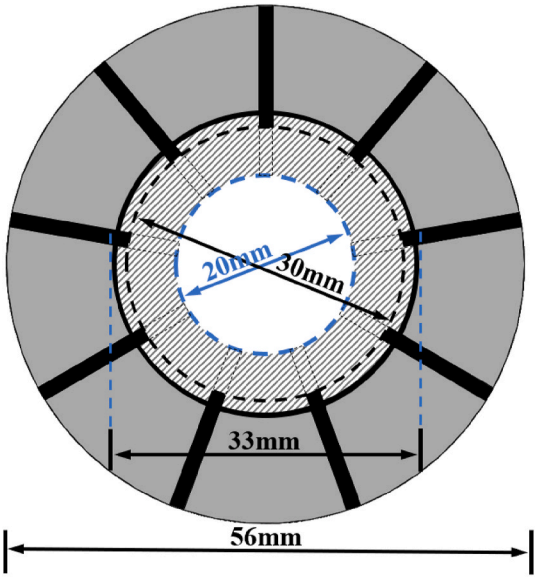

Fig. 3. Comparison of the A/PC grain cross-section before and after combustion.

where ρ_p and ρ_{ABS} are the densities of the PP and ABS, respectively, and ω_p and ω_{ABS} are the volume fractions occupied by the two materials not including the ABS outer wall of the A/PC grain. The change in the radius of the A/PC grain after combustion is illustrated in Fig. 3. Here, the shaded part represents the region consumed during the firing test, assumed to have an average density ρ_c.

The uncertainty, e_{total}, in the resulting regression rates had two components: that associated with measurement of the fuel grain mass, e_m, and that associated with determination of the burning time, e_t. The value of e_m was estimated to be 0.5%, based on the accuracy of the apparatus used for weighing, while e_t was less than 1% based on evaluation of the pressure-time traces. Thus, the value of e_{total} in the present

work was less than 1.23%.

3. Results and discussion

A total of 33 firing tests were conducted to investigate the coupling effect between the swirl injection and the composite fuel grain. All data from the engine tests conducted in this study are summarized in Table 1, including the initial oxygen mass flux, G_{ini}, average oxygen mass flux, G_{ave}, average combustion chamber pressure, P_c, average regression rate, r_{rate}, and average O/F values.

3.1. Variations in combustion chamber pressure

The combustion chamber pressure data provided valuable information regarding the operating state of each test. Fig. 4a plots the chamber pressure values over time for the four configurations as obtained with a constant initial oxygen mass flux of approximately 5.1 g/(s·cm^2). The timing of oxygen initiation and shutoff and engine ignition are also indicated in this plot, with the point at which the oxygen mass flow was initiated as time zero. The burn time, t_{burn}, was defined as the period between ignition and the cessation of the oxygen supply and P_c was determined over this time interval. Each plot demonstrates a rapid increase in the combustion chamber pressure following ignition at 2.0 s, indicating that all engines had similar ignition characteristics at the same initial oxygen mass flux. However, the combustion pressures during the trials with an A/PC grain and swirl injection were significantly higher than those observed during the firings using either the A/PC or PP grain together with axial injection. The combustion pressure obtained with the A/PC grain was also higher than that for the PP grain when using the conventional AF injector configuration. The increased pressures noted above are attributed to enhanced grain regression in all cases.

Fig. 4b also shows similar phenomena to Fig. 4a, and they are caused by the same reason. Notably, providing the same average oxygen mass flux required an increase in the initial oxygen mass rate as the grains regression rate increased for the different configurations. Both the increase in the grain regression rate and in the oxygen flow rate raised the combustion chamber pressure significantly. Furthermore, the discrepancies in ignition points among the four configurations were caused by the variations in the valve switching delay that in turn resulted from differences in the oxidizer flow rates.

3.2. Regression rates

3.2.1. Firing test results

The regression rate is a key characteristic of the solid fuel in a HRE and this parameter largely determines the thrust of the engine. The regression rate of grains $\dot{r}$ is often expressed as a function of G_{ox}:

$$\dot{r} = aG_{ox}^{n} \tag{4}$$

where a and n are constants obtained by fitting the experimental results and G_{ox} is the mass flux of the oxidizer.

Fig. 5 plots the regression rates obtained for the four configurations as functions of the average oxygen mass flux. The associated equations were

$$SD.injector\cdot\ +\cdot A/PC.gain:\cdot\dot{r} = 0.325G_{ox}^{1.09} \tag{5}$$

$$SD.injector\cdot\ +\cdot A/PC.gain:\cdot\dot{r} = 0.400G_{ox}^{0.81} \tag{6}$$

$$SD.injector\cdot\ +\cdot A/PC.gain:\cdot\dot{r} = 0.252G_{ox}^{0.84} \tag{7}$$

and

$$AF.injector\cdot\ +\cdot PP\cdot gain:\cdot\dot{r} = 0.291G_{ox}^{0.61} \tag{8}$$

As shown in Fig. 5, the regression rate of the A/PC grain when using

Table 1
Summary of firing test results.

No.	Engine configuration	G_{ini} g/(s·cm^2)	G_{ave} g/(s·cm^2)	Pc (MPa)	rate (mm/s)		O/F
1	SD injector + A/PC grain	3.06	2.15	1.01	0.73	1.80	
2		3.66	2.45	1.16	0.82	1.93	
3		4.30	2.70	1.41	0.96	1.86	
4		4.84	2.95	1.66	1.04	1.91	
5		5.76	3.19	1.86	1.26	1.78	
6		6.18	3.71	2.19	1.31	1.91	
7		6.46	3.89	2.16	1.43	1.81	
8		6.46	4.04	2.20	1.49	1.80	
9		6.81	4.14	2.20	1.52		1.83
10		7.16	4.15	2.38	1.5		1.90
11		7.54	4.24	2.58	1.55		1.90
12	OD injector + A/PC grain	3.25	2.27	1.05	0.75		1.90
13		3.72	2.59	1.21	0.76		2.16
14		4.49	2.86	1.44	0.95		2.00
15		5.22	3.13	1.62	1.03		2.06
16		5.79	3.36	1.85	1.16		2.00
17		6.21	3.65	2.13	1.20		2.12
18		6.43	4.12	2.10	1.23		2.20
19		7.13	4.50	2.33	1.28		2.30
20	AF injector + A/PC grain	3.00	2.30	0.84	0.54		2.56
21		3.69	2.83	1.02	0.56		3.00
22		4.36	3.17	1.23	0.64		3.04
23		4.33	3.25	1.20	0.62		3.20
24		5.19	3.46	1.39	0.76		2.91
25		5.09	3.54	1.45	0.76		2.93
26		5.82	3.94	1.70	0.82		3.06
27		6.68	4.47	1.76	0.86		3.36
28	AF injector + PP grain	2.67	2.28	0.76	0.52		2.54
29		3.01	2.77	0.82	0.54		2.80
30		3.69	3.37	0.97	0.60		3.16
31		4.39	3.74	1.18	0.66		3.30
32		5.16	3.81	1.36	0.68		3.39
33		5.92	4.42	1.52	0.71		3.80

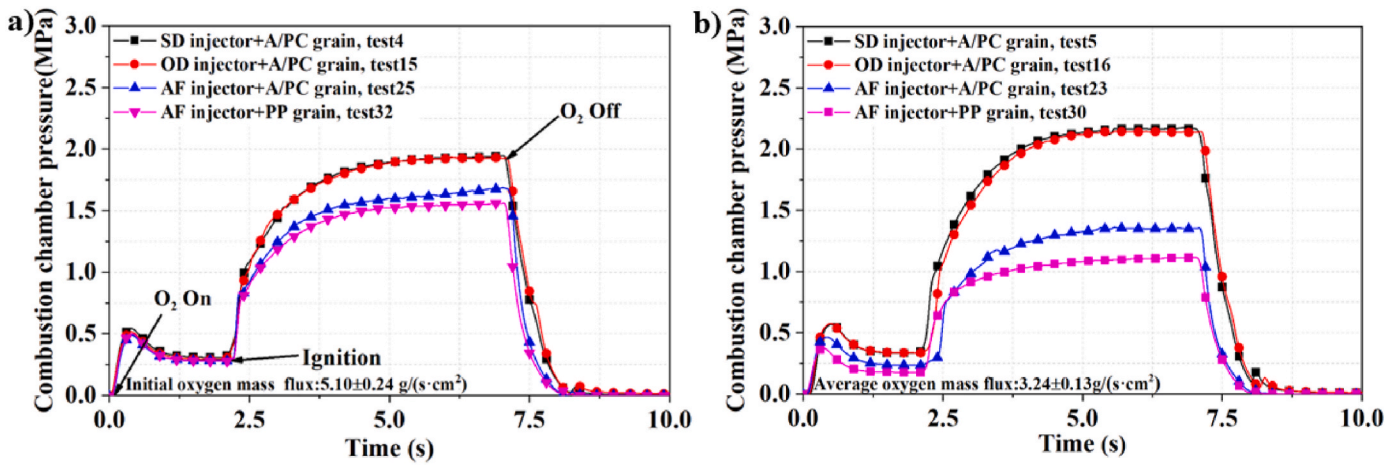

Fig. 4. Time histories of chamber pressures from typical firing tests conducted at a) the same initial oxygen mass flux and b) the same average oxygen mass flux.

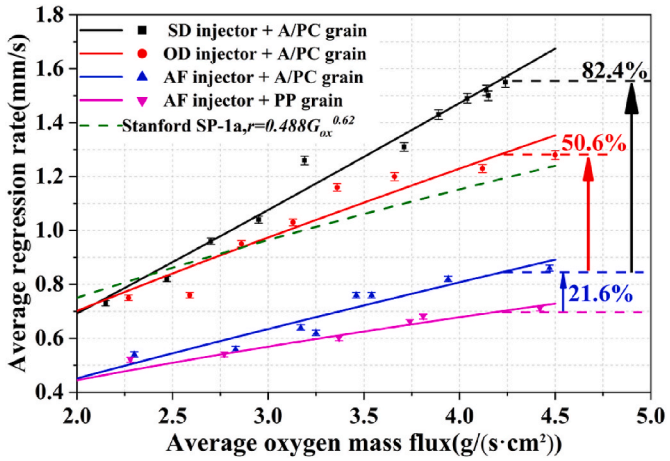

Fig. 5. Regression rates for the four engine configurations as functions of average oxygen mass flux.

axial injection was higher than that of the PP grain. At an oxygen mass flux of approximately 4.25 g/(s·cm^2), the regression rate of the A/PC grain was 21.6% greater than that of the PP grain. These results once again verified that the nested helical structure improved the regression rate. In addition, the regression rates of the A/PC grains when using the swirl flow injectors were greatly improved relative to the value observed with the AF injector. The regression rates of the A/PC grains were greatly increased at the lowest oxygen mass flux values and also increased more rapidly along with the oxygen mass flux compared with the results obtained using the AF injector. At an oxygen mass flux of approximately 4.25 g/(s·cm^2), the regression rates of the A/PC grains using the SD and OD injectors were 82.4% and 50.6% faster than that recorded using the AF injector, respectively. Interestingly, the regression rate of the A/PC grain in conjunction with the OD injector was lower than that obtained using the SD injector. It is possible that the nested helical structure reduced the intensity of the swirl flow field generated by the OD injector, and this effect is analyzed numerically in section 3.2.3.

Overall, it is evident that both types of swirl flow injector greatly enhanced the regression rate of the A/PC grain. In particular, the regression rate of the A/PC grain when using swirl injection exceeded that reported for the Stanford University SP-1a paraffin-based fuel grain [37] at oxygen mass flux values greater than approximately 2.85 g/(s·cm^2) (as indicated by the green dashed line in Fig. 5).

3.2.2. Inner surface imaging of the A/PC grains

The inner surfaces of the A/PC grains were evaluated using 3D imaging to explore the effects of different injectors on the nested helical structure. This imaging was typically performed by first cutting each grain longitudinally along the port centerline after a firing test. Following this, 3D scanning of the dissected grain was performed after which the resulting images were inverse modeled to obtain detailed dimensions. As shown in the red dashed panel within Fig. 6a, the groove depth, D_g, was used to characterize the grain, defined as the difference between the highest and lowest points of the corresponding cross-section. Fig. 6b–d present images of the groove cross-sections of three grains after combustion with the three different injectors at an oxygen mass flux of approximately 4.4 g/(s·cm^2). In this imaging process, six grooves (75% of the total number of grooves) close to the post combustion chamber were selected because the strong scouring effect of the flow generated by the swirl injector on the grains near the pre-combustion chamber was expected to distort the grooves in that region. The images in the blue chain line panels within Fig. 6b–d show the selected grooves while the red chain line panel parts show the damage to the groove morphology caused by swirling.

Fig. 7 summarizes the groove depth data obtained from Fig. 6b–d. The average groove depth of the A/PC grain when using the SD, OD and AF injectors was determined to be 1.46, 1.06 and 0.69 mm, respectively. Thus, the average groove depth was greater following trials with the swirl flow injectors. This possibly as a consequence of the stronger swirl flow field generated by the corresponding injector coupled with the nested helical structure. This phenomenon may also be an important reason for the sequence of regression rates. In addition, the groove depths of the two A/PC grains used in trials with the swirl flow injectors exhibited decreases along the flow direction, indicating that the swirling intensity generated by the injectors was attenuated moving along the engine axis. In contrast, the swirling intensity induced by the nested helical structure did not vary significantly along the engine axis, such that there were no significant variations in the depths of these grooves in the grains when using the AF injector.

3.2.3. Flow field analysis of different engine configurations

The ANSYS Fluent software package was used to investigate the internal flow fields of the grain ports for the different configurations. Although these cold flow numerical simulations were only approximate, they provided insights into the complicated flow morphology within the nested helical structure. On the basis of the results obtained using the 3D scanner, the groove depth was set to 1 mm and the inner diameter of the PP fuel was set to 27 mm during these simulations. To simplify the calculations, the groove cross-section was modeled using an annular sector. The geometric model for the SD injector coupled with the A/PC

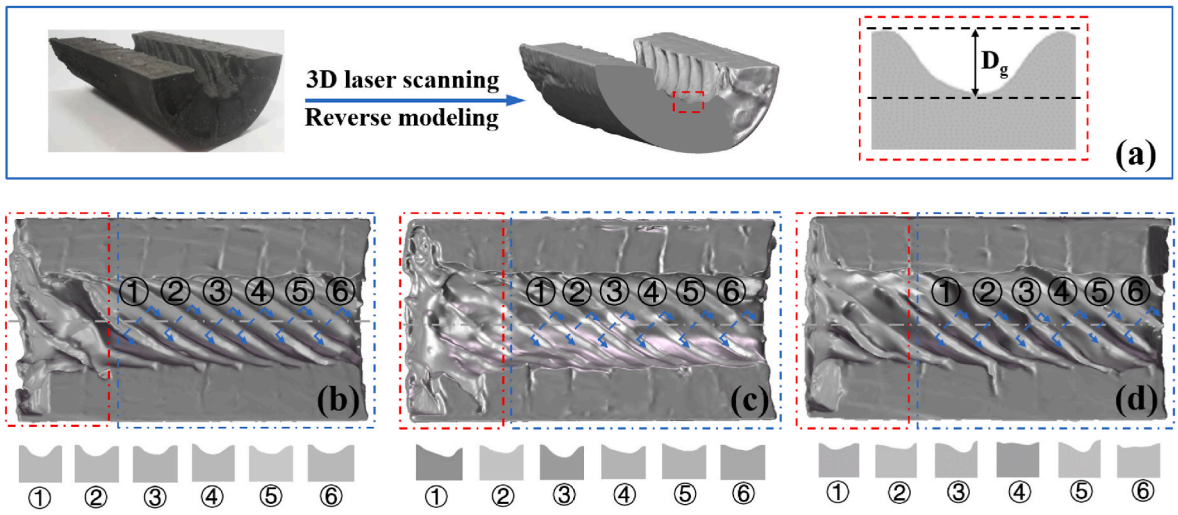

Fig. 6. (a) Definition of groove depth, D_g. Cross-sections of grooves in A/PC grains after combustion using (b) the SD injector, (c) the OD injector, and (d) the AF injector.

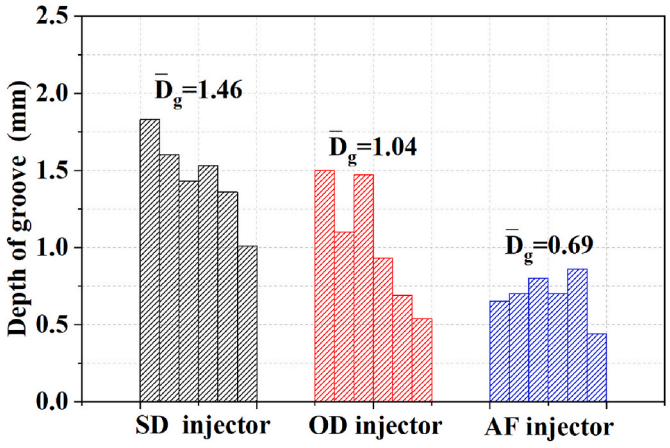

Fig. 7. The groove depths of AP/C grains using different injectors.

grain configuration is presented in Fig. 8.

The boundary conditions for these simulations were the mass flow inlet and pressure outlet, with the inlet to the domain considered to be uniform. The Navier-Stokes equations were solved using a steady-state pressure-based solver and the SST k-ε turbulence model was employed to model the turbulent flow field. Paraffin-based fuel was replaced with ethylene in these simulations to simplify the calculations (because paraffin consists of mixed saturated alkanes with a combustion process similar to that of ethylene [38]) and species transport equations were solved to determine the extent of mixing between the oxygen and ethylene flows in the computational domain. The maximum mass flow rate under our experimental conditions (test 11) was chosen as the input parameter, and the corresponding mass flow rate of oxygen and fuel were 23.6 g/s and 12.1 g/s, respectively. Because of the structural complexity of the helical groove in the present engine, unstructured 3D grids were utilized in the simulation. Three mesh sets were generated to model the SD injector coupled with the A/PC grain to ensure grid convergence, using 4, 6.5 and 9.5 million cells, respectively. A medium-level mesh comprising approximately 6.5 million cells was used in the subsequent modeling to reduce the computational cost while still obtaining suitably accurate results.

The surface streamline and velocity vector distributions for the four engine configurations at the A - A section are provided in Fig. 9. Comparing Fig. 9a and b shows that the A/PC grain combined with the AF injector generated a tangential velocity in the flow field, indicating the efficacy of the nested helical structure in terms of inducing swirling flow. From Fig. 9c and d, it is evident that the flow field velocity in the SD injector configuration was higher than that obtained using the OD injector configuration. This effect was ascribed to the weakening of the swirl flow field generated by the OD injector as a consequence of the nested helical structure. In addition, it can be seen from Fig. 9c that the streamlines generated by the SD injector configuration were denser near the grain inner surface because of the centrifugal force generated by the swirl injection. Two opposite tangential velocities can be observed in Fig. 9d, caused by the superposition of two opposing swirl flow fields. This effect would be expected to promote mixing of the oxidizer and fuel and so improve the combustion efficiency.

The effect of the flow in the engine on the grain regression rate was also examined by assessing the swirling intensity distribution along the Y-axis (as indicated by the black arrows at the A-A section in Fig. 8) of the selected section. The resulting data are plotted in Fig. 10. Note that

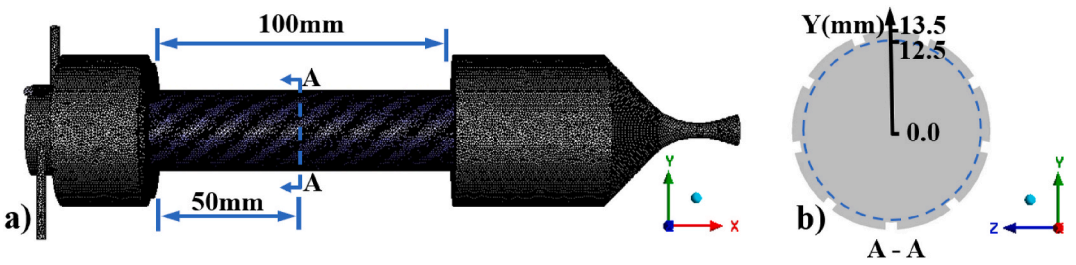

Fig. 8. a) A typical 3D computational mesh model for the engine inner flow field showing the location of the A - A section and b) a view of the A - A section indicating the Y-axis position.

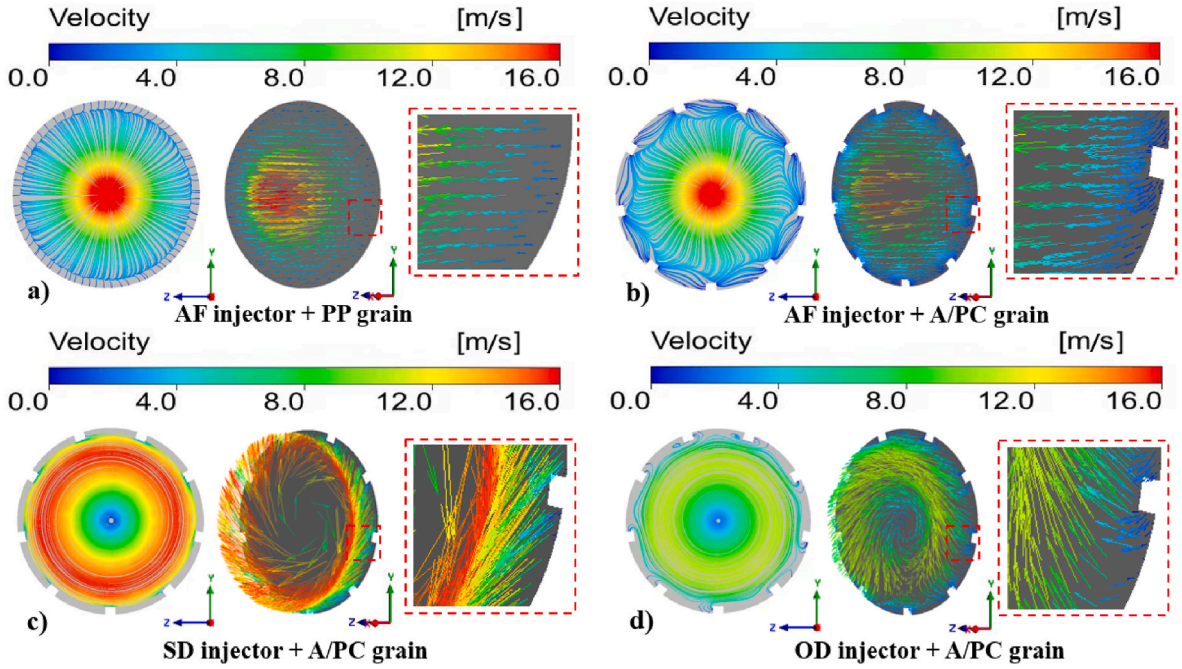

Fig. 9. Streamline and velocity vector diagrams for the a) AF injector + PP grain, b) AF injector + A/PC grain, c) SD injector + A/PC grain and d) OD injector + A/PC grain configurations.

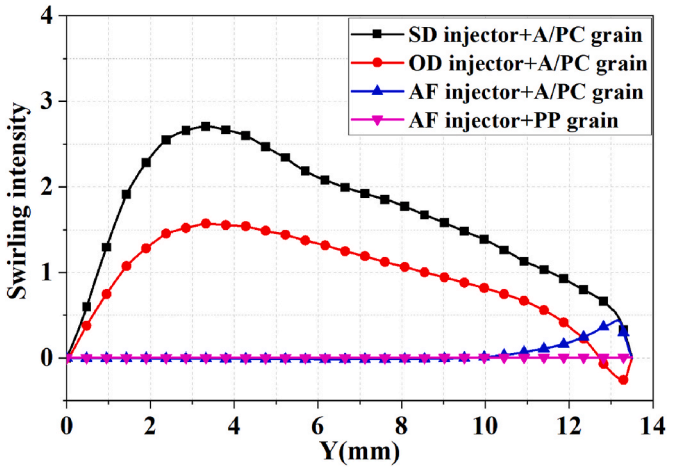

Fig. 10. Tangential velocity distributions along the Y-axis of section A-A for the different configurations.

the swirl flow field was very minimal in the combustion chamber of the engine using the PP grain, and so is not discussed here. It is obvious that the SD injector greatly increased the swirl intensity compared with the AF injector. This effect would increase turbulent intensity of the mixed airflow in the combustion chamber and thus be expected to improve the combustion efficiency. In addition, the centrifugal force brought the flame closer to the grain surface and the swirling flow produced a shearing effect at the grain's inner surface. These factors enhanced the heat and mass transfer between the combustion zone and the fuel wall and also increased droplet entrainment by the paraffin-based fuel. These are considered to be the main reasons why swirl injection increased the regression rate of the A/PC grain.

In the case of the OD injector, the swirl intensity of the flow field in the engine decreased rapidly and eventually became negative near the inner surface. This effect occurred as a consequence of the tangential velocity opposite to the injection direction of the OD injector that was induced by the nested helical structure. Compared with the engine incorporating the AF injector, the flow swirl intensity of the engine with the OD injector was lower near the inner surface. However, because of the thick boundary layer associated with the paraffin-based fuel during combustion [39], the swirl intensity throughout the entire combustion chamber played a more important role in determining the fuel combustion than that near the inner surface. This was likely the reason why the A/PC grain coupled with the OD injector exhibited a higher regression rate than that using AF injection. However, the combustion process complicates this issue and elucidation of the mechanism in detail will require further analysis.

3.3. Combustion efficiency and O/F distribution

Combustion efficiency is another important parameter by which the performance of an engine can be evaluated. It is usually expressed by the ratio of the experimental characteristic velocity over the theoretical characteristic velocity:

$$\eta = \frac{C_e^*}{C_t^*} \tag{9}$$

Among them the experimental characteristic velocity, C_a*, is expressed as:

$$C_e^* = \frac{P_c A_t}{\dot{m}} \tag{10}$$

where A_t and $\dot{m}$ are the nozzle throat area and average mass flow of propellant, respectively. Theoretical characteristic velocities, C_t*, calculated by the Chemical Equilibrium with Applications software (CEA). Fig. 11 summarizes the combustion efficiency data obtained for the four engine configurations, all of which were within the range of 71%–78%. The combustion efficiency of the A/PC grains combined with the swirl flow injectors were not improved relative to that combined with the AF injector, possibly as a consequence of the low O/F values that resulted from the greatly increased grain regression rates. It is likely that the combustion efficiency of the A/PC grains when using the swirl flow injectors could be improved by increasing the O/F because higher O/F values would increase the exposure of the fuel droplets to the oxidizer [37,40].

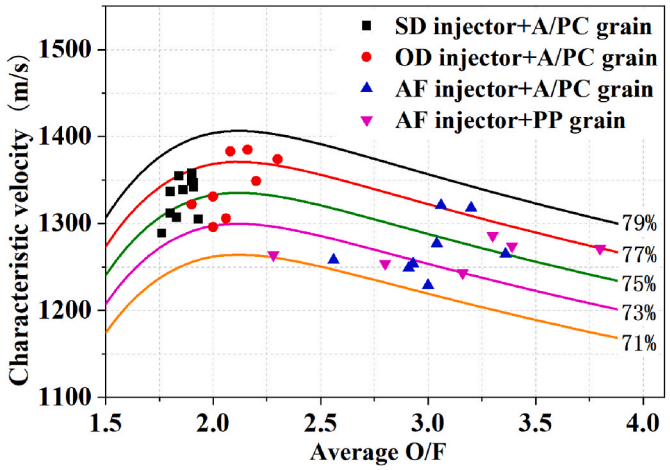

Fig. 11. Combustion efficiency and O/F distributions for the four configurations.

Interestingly, the significant increase in the grain regression rates also resulted in more concentrated O/F distributions. In the case of an HRE, the O/F can vary during operation because of continuous changes in the fuel regression rate caused by variations in the oxygen mass flux. In real-world applications, such O/F shifts would reduce the performance of the engine and increase the launch cost [41]. Fig. 11 shows that the injection methods had a pronounced effect on the O/F distribution range. As an example, the O/F range of the novel composite grain when using the SD injector was only 0.13. Therefore, it would be helpful to explore the effect of the injector on the O/F shift of the A/PC grain in conjunction with changes in the oxygen mass flux. According to the empirical regression rate fitting formula (Eq. (4)), the average fuel mass flow rate, $\dot{m}_f$, will be a function of the average oxygen mass flux, G_{ox}, according to the relationship

$$\dot{m}_f = \frac{[\pi(t_{ave}\cdot aG_{ox}^n + r_0)^2 - \pi r_0^2]L\rho}{t_{ave}} \tag{11}$$

where t_{ave} is the average burning time for a given configuration. Similarly, the average oxygen mass flow rate, $\dot{m}_{ox}$, can be expressed based on the average oxygen mass flux as

$$\dot{m}_{ox} = G_{ox}\cdot\pi(t_{ave}\cdot aG_{ox}^n + 2r_0)^2 \Big/ 4 \tag{12}$$

Finally, O/F can be written as

$$O\Big/F = \frac{\dot{m}_{ox}}{\dot{m}_f} = \frac{G_{ox}(a^2t_{ave}^2G_{ox}^{2n} + 4at_{ave}r_0G_{ox}^n + 4r_0^2)}{4L\rho(a^2t_{ave}G_{ox}^{2n} + 2ar_0G_{ox}^n)} \tag{13}$$

Fig. 12 plots O/F values as functions of the average oxygen mass flux, from which it is evident that the O/F shift of the A/PC grain with changes in the average oxygen mass flux was less than that of the PP grain. It is noteworthy that the O/F shift was also significantly reduced in the case that an A/PC grain was paired with swirl injection. The data obtained using the SD injector coupled with an A/PC grain are approximately parallel to the X-axis, demonstrating that the O/F value was almost constant under the present experimental conditions. This result could be important to the future development of methods to control the O/F values of HREs.

In general, the present results confirm that swirl injection greatly increased the regression rate of the A/PC grain and also assisting in tuning the O/F value of the engine. The mechanism by which the regression rate was increased was evaluated based on imaging of the inner surface of the grain and cold flow numerical simulations. Future investigations by our group will focus on the effect of the swirling intensity of the flow field generated by injectors on the combustion

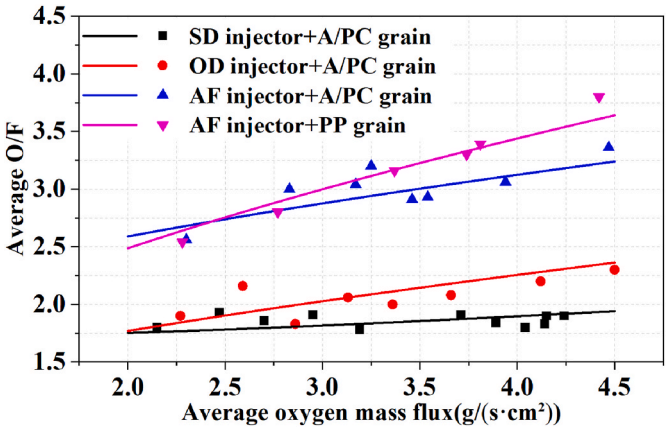

Fig. 12. Average O/F values as functions of the average oxygen mass flux.

characteristics of the A/PC grain. Injectors with different swirl numbers will also be added to the combustion experiments. This research will involve numeral calculations [42] based on more complex numerical models taking into account the coupling between chemical kinetics and radiation.

4. Conclusions

The combustion characteristics of an A/PC grain combined with swirl injectors were studied. The data that were considered included the combustion chamber pressure, regression rate, combustion efficiency and O/F distribution. Using 3D scanner imaging and cold flow numerical simulations, the mechanism by which the regression rate was enhanced was analyzed. The conclusions obtained in this study can be summarized as follows.

(1) Swirl injection can effectively improve the regression rate of an A/PC grain. The SD and OD injectors both increased the regression rate of the A/PC grain, by 82.4% and 50.6% respectively, at an oxygen mass flux of 4.25 g/(s·cm^2) compared with the results obtained using the axial flow injector.
(2) Swirl injection is conducive to the formation of grooves in the A/PC grain and swirl injection combined with deeper grooves may further increase the grain regression rate.
(3) Numerical simulation results showed that the flow field swirl intensity of the A/PC grain when using the SD injector was significantly higher than that using the OD injector, which may have been the primary reason for the different regression rates exhibited by the A/PC grains.
(4) The combined effect of swirl injection and the novel composite grain morphology provided approximately constant O/F values under the present experimental conditions. This phenomenon could permit precise control over the combustion of HREs and should be further explored in the future.

Declaration of competing interest

The authors declare that they have no known competing financial interests or personal relationships that could have appeared to influence the work reported in this paper.

Acknowledgement

This work was supported by the National Natural Science Foundation of China (No. 11802315, 12072355, 11872368 and 11927803), Key-Area Research and Development Program of Guangdong Province (No.2021B0909060004), National Key Project (No. GJXM92579), and

the Youth Innovation Promotion Association of CAS (No. 2022018).

References

[1] H. Tian, Y. Duan, H. Zhu, Three-dimensional numerical analysis on combustion performance and flow of hybrid rocket motor with multi-segmented grain, Chin. J. Aeronaut. 33 (2020) 1181–1191, https://doi.org/10.1016/j.cja.2019.12.021.

[2] H. Tian, Y. Li, P. Zeng, Transient simulation of regression rate on thrust regulation process in hybrid rocket motor, Chin. J. Aeronaut. 27 (2014) 1343–1351, https://doi.org/10.1016/j.cja.2014.08.016.

[3] G. Cai, B. Cao, H. Zhu, et al., Parametric investigation of secondary injection in post-chamber on combustion performance for hybrid rocket motor, Acta Astronaut. 140 (2017) 427–438, https://doi.org/10.1016/j.actaastro.2017.09.009.

[4] L. Luca, T. Shimada, V.P. Sinditskii, et al., Chemical Rocket Propulsion, Springer, Berlin, 2017.

[5] K.K. Kuo, M.J. Chiaverini, Fundamentals of Hybrid Rocket Combustion and Propulsion, AIAA, Reston, 2007.

[6] H. Zhu, H. Tian, G. Cai, et al., Uncertainty analysis and design optimization of hybrid rocket motor powered vehicle for suborbital flight, Chin. J. Aeronaut. 28 (2015) 676–686, https://doi.org/10.1016/j.cja.2015.04.015.

[7] E.T. Jens, B.J. Cantwell, G.S. Hubbard, Hybrid rocket propulsion systems for outer planet exploration missions, Acta Astronaut. 128 (2016) 119–130, https://doi.org/10.1016/j.actaastro.2016.06.036.

[8] W.H. Knuth, M.J. Chiaverini, J.A. Sauer, et al., Solid-fuel regression rate behavior of vortex hybrid rocket engines, J. Propul. Power 18 (2002) 600–609, https://doi.org/10.2514/2.5974.

[9] S. Yuasa, O. Shimada, T. Imamura, et al., A technique for improving the performance of hybrid rocket engines, in: 35th Joint Propulsion Conference and Exhibit, 1999, https://doi.org/10.2514/6.1999-2322.

[10] S. Ohyama, S. Aso, Y. Hirata, et al., A study of hybrid rockets with multi-section swirl injection method, in: 48th AIAA/ASME/SAE/ASEE Joint Propulsion Conference & Exhibit, 2012, https://doi.org/10.2514/6.2012-3905.

[11] S. Ohyama, Y. Hirata, K. Araki, et al., Effects of multi-section swirl injection method on fuel regression rate of high density polyethylene fueled hybrid rocket engine, in: 49th AIAA/ASME/SAE/ASEE Joint Propulsion Conference, 2013, https://doi.org/10.2514/6.2013-4040.

[12] Y. Hirata, S. Aso, T. Hayashida, et al., Improvement of regression rate and combustion efficiency of high density polyethylene fuel and paraffin fuel of hybrid rockets with multi-section swirl injection method, in: 47th AIAA/ASME/SAE/ASEE Joint Propulsion Conference & Exhibit, 2011, https://doi.org/10.2514/6.2011-5907.

[13] S. Aso, Y. Tani, T.S. Saiga, et al., A study on high performance hybrid rocket engine with multi-section swirl injection method for space propulsion system, in: AIAA Aerospace Sciences Meeting, 2018, https://doi.org/10.2514/6.2018-1415, 2018.

[14] T. Sakurai, S. Yuasa, H. Ando, et al., Performance and regression rate characteristics of 5-kN swirling-oxidizer-flow-type hybrid rocket engine, J. Propul. Power 33 (2017) 891–901, https://doi.org/10.2514/1.B36239.

[15] M. Franco, F. Barato, E. Paccagnella, et al., Regression rate design tailoring through vortex injection in hybrid rocket motors, J. Spacecraft Rockets 57 (2020) 278–290, https://doi.org/10.2514/1.A34539.

[16] H. Tada, S. Aso, Y. Tani, et al., Visualization of flames in combustion chamber of hybrid rocket engine with multi-section swirl injection method, in: 50th AIAA/ASME/SAE/ASEE Joint Propulsion Conference, 2014, https://doi.org/10.2514/6.2014-3850.

[17] N. Bellomo, F. Barato, M. Fenaza, et al., Numerical and experimental investigation of unidirectional vortex injection in hybrid rocket engines, J. Propul. Power 29 (2013) 1097–1113, https://doi.org/10.2514/1.B34506.

[18] W. Li, X. Chen, D. Zhao, et al., Swirling effect on thermodynamic performance in a solid fueled ramjet with paraffin-polyethylene, Aero. Sci. Technol. 107 (2020), https://doi.org/10.1016/j.ast.2020.106341.

[19] C. Li, G. Cai, H. Tian, Numerical analysis of combustion characteristics of hybrid rocket motor with multi-section swirl injection, Acta Astronaut. 123 (2016) 26–36, https://doi.org/10.1016/j.actaastro.2016.02.023.

[20] I. Nakagawa, D. Kishizato, Y. Koinuma, et al., Demonstration of an altering-intensity swirling-oxidizer-flow-type hybrid rocket function, J. Propul. Power 37 (2021) 326–331, https://doi.org/10.2514/1.B37915.

[21] F.D. Quadros, P.T. Lacava, Swirl injection of gaseous oxygen in a lab-scale paraffin hybrid rocket motor, J. Propul. Power 35 (2019) 896–905. https://doi:10.2514/1.B37283.

[22] S.A. Whitmore, S.D. Walker, D.P. Merkley, et al., High regression rate hybrid rocket fuel grains with helical port structures, J. Propul. Power 31 (2015) 1727–1738, https://doi.org/10.2514/1.B35615.

[23] S.A. Whitmore, S.D. Walker, Engineering model for hybrid fuel regression rate amplification using helical ports, J. Propul. Power 33 (2017) 398–407, https://doi.org/10.2514/1.B36208.

[24] J.H. Marshall, S.A. Whitmore, M. Heiner, Thrust augmented nozzle for a hybrid rocket with a 3-D printed helical fuel grain, in: 53rd AIAA/SAE/ASEE Joint Propulsion Conference, 2017, https://doi.org/10.2514/6.2017-4983.

[25] J. Catina, B. Nellis, L.D. Grigsby, et al., Use of additive manufacturing to develop advanced hybrid rocket designs, in: 52nd AIAA/SAE/ASEE Joint Propulsion Conference, 2016, https://doi.org/10.2514/6.2016-4506.

[26] L. Pabarcius, Development and preliminary testing of paraffin hybrid rocket fuel grains with helical port structures, in: AIAA Propulsion and Energy 2019 Forum, 2019, https://doi.org/10.2514/6.2019-4187.

[27] J. McCulley, A.R. Bath, S. Eilers, et al., Design and testing of FDM manufactured paraffin-ABS hybrid rocket motors, in: 48th AIAA/ASME/SAE/ASEE Joint Propulsion Conference & Exhibit, 2012, https://doi.org/10.2514/6.2012-3962.

[28] K.H. Shin, C.J. Lee, S.J. Chang, et al., The enhancement of regression rate of hybrid rocket fuel by various methods, in: 43rd AIAA Aerospace Sciences Meeting and Exhibit, 2005, https://doi.org/10.2514/6.2005-359.

[29] C. Lee, Y. Na, G. Lee, The enhancement of regression rate of hybrid rocket fuel by helical grain configuration and swirl flow, in: 41st AIAA/ASME/SAE/ASEE Joint Propulsion Conference & Exhibit, 2005, https://doi.org/10.2514/6.2005-3906.

[30] C. Lee, Y. Na, Y.C. Hwang, et al., Turbulent flow in the helical grain of hybrid rocket fuel, in: 42nd AIAA/ASME/SAE/ASEE Joint Propulsion Conference & Exhibit, 2006, https://doi.org/10.2514/6.2006-4344.

[31] H. Tian, Y. Li, C. Li, et al., Regression rate characteristics of hybrid rocket motor with helical grain, Aero. Sci. Technol. 68 (2017) 90–103, https://doi.org/10.1016/j.ast.2017.05.006.

[32] Z. Wang, X. Lin, F. Li, et al., Combustion performance of a novel hybrid rocket fuel grain with a nested helical structure, Aero. Sci. Technol. 97 (2020), 105613, https://doi.org/10.1016/j.ast.2019.105613.

[33] Y. Wu, X. Yu, X. Lin, et al., Experimental investigation of fuel composition and mix-enhancer effects on the performance of paraffin-based hybrid rocket motors, Aero. Sci. Technol. 82 (2018) 620–627, https://doi.org/10.1016/j.ast.2018.09.026.

[34] Z. Wang, X. Lin, F. Li, et al., Improving the combustion performance of a hybrid rocket engine using a novel fuel grain with a nested helical structure, J. Vis. Exp. 167 (2021), https://doi.org/10.3791/61555.

[35] X. Lin, D.D. Qu, X.D. Chen, et al., Three-dimensional printed metal-nested composite fuel grains with superior mechanical and combustion properties, Virtual Phys. Prototyp. 17 (2022) 437–450. https://doi:10.1080/17452759.2022.2035934.

[36] G. Cai, Z. Zhao, B. Zhao, et al., Regression rate and combustion performance investigation on hybrid rocket motor with head-end swirl injection under high geometric swirl number, Aero. Sci. Technol. 103 (2020), 105922, https://doi.org/10.1016/j.ast.2020.105922.

[37] A. Karabeyoglu, G. Zilliac, B.J. Cantwell, et al., Scale-up tests of high regression rate paraffin-based hybrid rocket fuels, J. Propul. Power 20 (2004) 1037–1045, https://doi.org/10.2514/1.3340.

[38] L. Liu, X. He, Y. Wang, et al., Regression rate of paraffin-based fuels in hybrid rocket motor, Aero. Sci. Technol. 107 (2020), 106269, https://doi.org/10.1016/j.ast.2020.106269.

[39] T.J. Elizabeth, C.K. Ashley, A.M. Victor, et al., Experimental visualization of hybrid combustion: results at elevated pressures, J. Propul. Power 36 (2020) 33–46, https://doi.org/10.2514/1.B37416.

[40] S. Fang, Z. Wang, X. Lin, et al., Characterizing combustion of a hybrid rocket using laser absorption spectroscopy, Exp. Therm. Fluid Sci. 127 (2021), 110411, https://doi.org/10.1016/j.expthermflusci.2021.110411.

[41] I. Nakagawa, D. Kishizato, Y. Koinuma, et al., Demonstration of an altering-intensity swirling-oxidizer-flow-type hybrid rocket function, J. Propul. Power 37 (2021) 326–331, https://doi.org/10.2514/1.B37915.

[42] Z. Wang, X. Lin, F. Li, et al., Determining the time-resolved mass flow rates of hybrid rocket fuels using laser absorption spectroscopy, Acta Astronaut. 188 (2021) 110–120, https://doi.org/10.1016/j.actaastro.2021.07.028.